A Study of the Gluon Propagator in SU(2) Lattice Gauge Theory

F. Gutbrod
Deutsches Elektronen-Synchrotron DESY

Notkestr. 85, D22603 Hamburg, Germany
e-mail: gutbrod@mail.desy.de

Abstract

The SU(2)-gluon propagator in Landau gauge (without fermions) and in momentum space is investigated on very large lattices. Boundary conditions are twisted ones. At large momenta, we find a region where 2-loop perturbation theory provides an excellent description of the data. The transition to the nonperturbative region is studied. Extrapolations to zero momentum yield a finite, nonzero propagator, with a pronounced nonlinear behaviour for the inverse propagator. This excludes a description by a single mass term. Attention is paid to the dependence of the propagator on different gauging algorithms. Scaling under different actions is studied, with small, but significant scaling violations. Gauged configurations, more precisely several field variables on a 2-dimensional lattice plane, have been visualized. The emerging graphs give support to the stochastic domain picture.

1 Introduction

Many physical quantities can be calculated in lattice gauge theory without using a specific gauge. Nevertheless it is believed that insight into the confinement mechanism of QCD and, more generally, into the nature of the vacuum is best obtained after transforming lattice gauge field configurations to some smooth gauge and by studying space-time correlations between gauge fields. The simplest quantity in this context is the gluon propagator, and in this paper it will be determined in pure SU(2) lattice gauge theory in Landau gauge.

One of the most interesting questions is the behaviour of the momentum space propagator at small momenta, for which there exists a wide spectrum of theoretical predictions or speculations. It ranges from a behaviour which is more singular than the simple pole of tree level perturbation theory on the one hand [1, 2, 3, 4, 5] to a vanishing propagator on the other [6, 7, 8]. The first case, equivalent to strong positive long range correlations, seems to get support by a perturbatively motivated connection between the Fourier transformed propagator and a linearly rising static $q\overline{q}$-potential. This connection is, however, not quite clear at large distances where physics may resemble the strong coupling regime. There also correlation functions higher than the simple two-point functions are relevant. The second case also implies long range correlations, but negative ones: The local fluctuations of gauge fields have to average to zero on large scales. Again this does not look very natural in euclidean lattice gauge theory where ordering at large distances is restricted to special situations like deconfinement above the finite temperature phase transition.

Another framework which can be relevant for the large distance behaviour is the stochastic domain picture of the QCD vacuum [9, 10]. There the long distance correlations are strongly damped, the zero momentum propagator being finite as a consequence

of statistical fluctuations. A finite propagator has also been advocated, on more phenomenological grounds, for constructing a Pomeron via gluon exchange [11, 12].

On the opposite side of the momentum spectrum, the approach to the perturbative regime is of interest. After all, asymptotic freedom of QCD has initially been derived for the propagators of gluons and quarks in Landau gauge [13, 14], and both the verification of the correct asymptotic decrease (relative to the tree level propagator) as well as the onset of nonperturbative contributions should be demonstrated clearly. Since the gluon propagator can be 'measured' on the lattice over a very large region in momentum space, the quality of this demonstration is perhaps quite unique. The region where nonperturbative effects become important is e.g. relevant for the determination of the strength of the gluon condensate [15, 16].

From lattice studies, evidence is accumulating [17, 18, 19, 20, 21, 12] that the propagator approaches simply a nonzero constant for euclidean momenta $p^2 \to 0$. This trend can hardly be described by a massive particle propagator since the inverse propagator is far from being linear in p^2. It is the aim of this paper to study the behaviour of the propagator somewhat more systematically, paying attention to the various difficulties encountered in its determination. The results to be presented here are fully compatible with previous findings.

The difficulties are the following: First of all, the gauging procedure is plagued by Gribov ambiguities [6], at least in practice and on large lattices. There is no certainty that the most interesting behaviour of the momentum space propagator, its constancy at small momenta, is not an artifact of 'insufficient' gauging, i.e. ending up in a local minimum with a less than minimal gauge function. A satisfactory solution to this problem is not in sight. We can only study the propagator for various gauging algorithms and as a function of the resulting gauge function. In this paper, some studies of of the Gribov problem have been undertaken by comparing four gauging algorithms on medium sized lattices. No significant differences between gauging by a simulated annealing algorithm, by overrelaxation in two variants and by a conjugate gradient algorithm have been found. A consistent scenario is thus that average properties in all local minima look similar, independent of the gauge function and that none of the algorithms has a particularly good chance of finding a global minimum.

Secondly, the low momentum propagator may be influenced by boundary conditions. Especially under periodic boundary conditions the zero momentum modes are suspicious, as the perturbative expansion is quartic in their amplitudes [22]. Whether there is a strong coupling of these anomalous amplitudes to other momentum amplitudes which might distort the propagator away from $p^2 = 0$ is an open question. In any case, it seems prudent to eliminate the zero modes by imposing twisted boundary conditions[23]. With those b.c. no significant influence of the lattice size on the propagator has been found, with lattice sizes ranging up to $48^3 \times 80$. The main lattice size effect is the varying infrared cut-off due to the lattice size. This has some implications on the Gribov problem. The number of possible minima, at least of those which can be found by iterative numerical algorithms, strongly depends on the lattice size. On small lattices, all algorithms end up in the same minimum. The fact that the propagator is insensitive to the lattice size and thus to the amount of ambiguity, provides additional indication that its small momentum behaviour is not a gauging artifact.

Finally, the scaling behaviour of the propagator as a function of the bare coupling constant has to be studied as well as its independence on the action, both in the infrared

and in the perturbative region.

At large momenta and for $\beta = 4/g_0^2 \geq 3.0$, a perturbative description of the propagator with a running coupling constant in 2-loop accuracy is seen to be valid on the level of 1 % or better. When lowering β at fixed momentum, one observes a quasi-exponential increase beyond perturbation theory. At fixed g_0^2, when going to smaller momenta, there is a similarly strong increase beyond the 2-loop perturbative result. It is extremely interesting to observe the fate of this increase. A qualitative description of this behaviour is that the propagator at a momentum of roughly 1 GeV rather abruptly deviates from a inverse power increase, i.e. the propagator divided by the bare one shows a clear break. A tentative interpretation of this phenomenon is that vacuum fluctuations exceeding a critical size are unstable and do not occur with significant probability. The propagator at $p^2 = 0$ then simply reflects the fluctuation of the number and strength of domains in a given lattice configuration.

Scaling tests have been performed both for fixed actions by varying β, and by changing the action via introducing anisotropic couplings for space-like and time-like directions. Scaling tests are more complicated for gauge dependent quantities, as compared e.g. for physical masses, due to β-dependent renormalization constants. Thus all statements depend on the assumption that the renormalization constant depends only weakly on β. This assumption can be checked in the perturbative region and it seems to be valid. Under this assumption, only weak scaling violations have been observed up to now, which have a similar pattern in three independent tests, thus strengthening the significance of the overall picture. With small variations of the renormalization constant, perfect scaling can be obtained.

The gluon propagator does not contain enough information to fully reconstruct the space-time picture on the lattice. It does not describe how various colour components are spatially connected, e.g. whether they cluster together, and how thick transition regions interpolate between possibly existing domains. In principle such problems can be studied more naturally in a visualization of actual lattice configurations. Because of the high dimensionality of non-abelian theories, this is a formidable task. A first step in this direction however gives evidence for domain formation, after the short range quantum noise is removed e.g. by Fourier filtering.

2 The Gluon Propagator on the Lattice

In this section I will collect the definitions for the propagator and report on the perturbative lattice calculations. The latter will be performed also for anisotropic lattices. Such lattices provide us with an extra handle for studying the dependence of the propagator on external parameters and improving confidence that the Monte Carlo results to be reported, are not artifacts of insufficient gauging.

2.1 Anisotropic Lattices

Throughout I will work with the representation

$$U_\mu(x) = u_0 + \frac{iag_0}{2}\vec{\tau}\vec{A}_\mu(x) \equiv u_0 + i\vec{\tau}\vec{u}_\mu(x). \tag{1}$$

This departure from the standard exponentiation of the $A-$fields is chosen in order to preserve the Landau gauge condition, which will be enforced on the Monte Carlo lattice

$U-$variables, to all orders in perturbation theory. It will lead to a different measure contribution in the one-loop perturbative expression.

Anisotropic lattices may be defined by changing the coupling constant in the Wilson action for time-like plaquettes. This modification can be removed by scale transformations, which may work as a tool to study scale invariance without increasing the lattice sizes too strongly. In detail, the modified lattice Wilson action is

$$S = \beta \, (\sum_{space} + \xi^2 \sum_{time}) \frac{tr}{2} (1 - \prod_{plaq} U_i). \tag{2}$$

In order to recognize the scale transformations connected with the anisotropy factor ξ^2, we have to make the substitution for the fields

$$\vec{A}_0(x) \to \vec{A}'_0(x) = \xi \vec{A}_0(x), \tag{3}$$

and for the time-like lattice derivative

$$\Delta_0 \to \Delta'_0 = \xi \Delta_0 \tag{4}$$

The Landau gauge condition is

$$\xi^2 \Delta_0 \vec{u}_0(x) + \sum_{i=1,3} \Delta_i \vec{u}_i(x) = \Delta'_0 \vec{u}'_0(x) + \sum_{i=1,3} \Delta_i \vec{u}_i(x) = 0. \tag{5}$$

At small momenta, the tree-level action is unchanged (see next subsection) after the substitution

$$p_0 \to p'_0 = \xi p_0, \tag{6}$$

as well as the non-abelian terms in the action at small momenta. However, the momentum integrals for one-loop Greens functions pick up a factor ξ^{-1} from the time integration. Thus, the logarithmic contributions are modified by a factor ξ^{-1}. This factor can be absorbed into a redefinition of the coupling constant. Furthermore, outside the infrared region, the action has a different momentum dependence, and the lattice-cut-off dependent contributions give an extra ξ-dependence which have to be calculated numerically.

2.2 The Propagator in Momentum Space

Fourier transformed $SU(2)$-fields are defined by (V = lattice volume)

$$\vec{u}_\mu(x) = \frac{1}{\sqrt{V}} \sum_p \vec{u}_\mu(p) e^{ip(x + e_\mu/2)}. \tag{7}$$

The allowed momenta depend on the boundary conditions, which are periodic ones in the time direction, leading to (for L_0 lattice sites in $t-$direction)

$$p_{0,n} = \frac{2\pi n}{L_0}, \quad n = 0, ..., L_0 - 1. \tag{8}$$

In all space directions twisted ones are used [23], which are

$$\begin{aligned} u^a_\mu(x + e_b L_b) &= u^a_\mu(x) \text{ for } a = b \text{ and } a = 1,2,3, \\ u^a_\mu(x + e_b L_b) &= -u^a_\mu(x) \text{ for } a \neq b. \end{aligned} \tag{9}$$

In the case of a sign flip, i.e. $b \neq a$, they lead to the momenta

$$p_{b,n} = \frac{2\pi(n + 1/2)}{L_b}, \quad n = 0, ..., L_0 - 1. \tag{10}$$

The absence of the zero momentum mode should make the propagator less sensitive to the effects of finite lattice sizes [23].

The tree level action is

$$S_0 = \frac{1}{2}\sum_{p_0,p_i}[A_0'(p)A_0'(-p) + \sum_{i=1,3} A_i(p)A_i(-p)](\xi^2\hat{p}_0^2 + \sum_{i=1,3}\hat{p}_i^2), \tag{11}$$

with $\hat{p}_\mu = 2\sin\frac{p_\mu}{2}$.

The gluon propagator in x-space will be defined [1] as

$$G_{\mu\nu}(x) = \frac{1}{3V}\sum_y < \vec{A}_\mu(y)\vec{A}_\nu(y+x) >= \frac{4}{3g_0^2a^2V}\sum_y < \vec{u}_\mu(y)\vec{u}_\nu(y+x) > . \tag{12}$$

In momentum space we have

$$G_{\mu\nu}(p) = \sum_x e^{-ipx}G_{\mu\nu}(x) = \frac{1}{3} < \vec{A}_\mu(p)\vec{A}_\mu(-p) > . \tag{13}$$

For isotropic lattices and for small momenta, where lattice artifacts have little influence(see e.g. [24]), the gluon propagator in Landau gauge has the form

$$G_{\mu\nu}(p) = (\delta_{\mu\nu} - \frac{p_\mu p_\nu}{p^2})G(p^2). \tag{14}$$

It is natural to define the scalar part of the propagator also for larger momenta as

$$G(\hat{p}^2) = \frac{1}{3}\sum_{\mu=0,3} G_{\mu\mu}(p). \tag{15}$$

For anisotropic lattices, we note that the tree-level rescaling, according to eqs. 3 and 4, leads to a form of the propagator identical to eq. 14, if expressed in terms of the $\vec{A}'$-fields and of the scaled four momentum p'. In addition, however, there are quantum corrections [25] to the scale of the time-like momentum w.r.t. the space-like momentum, which require a more general connection between $\hat{p}$ and $\hat{p}'^2$. This will be discussed in more detail below.

Returning to the definition 12 of the anisotropic lattice propagator, I thus assume the form

$$G_{\mu\nu}(p) = (\xi_{\mu\nu} - \frac{\hat{p}_\mu\hat{p}_\nu}{\hat{p'}^2})G(\hat{p}'^2) \tag{16}$$

with $\xi_{\mu\nu}$ given by

$$\xi_{00} = \xi^{-2} \quad \text{and} \quad \xi_{\mu\nu} = \delta_{\mu\nu} \quad \text{otherwise}, \tag{17}$$

and with rescaled momentum

$$\hat{p}'^2 = \lambda_{st}\xi^2\hat{p}_0^2 + \vec{\hat{p}}^2 . \tag{18}$$

The extra quantum scaling factor λ_{st} will be determined in the next subsection. The scalar part of the propagator in the anisotropic case is then

$$G(\hat{p}'^2) = \frac{1}{3}[\xi^2 G_{00}(p') + \sum_{i=1,3} G_{ii}(p')]. \tag{19}$$

With this definition, the scalar propagator will be determined both by Monte Carlo and by 1-loop perturbation theory.

[1] This definition leads to no explicit volume dependence, in contrast to the normalization used in [20].

2.3 One-loop Perturbation Theory

Lattice perturbation theory, especially for anisotropic lattices and for complicated gauges such as eq. 5, is not particularly pleasant. I have therefore tried to do the functional integral by generating random fields $A_\mu(p)$ which are transverse in the sense of eq. 5, with a probability according to the zeroth order action eq. 11. After transformation to $x-$space, the calculation of the higher orders of the action and of the Fadeev-Popov determinant is straightforward. In order to obtain sufficient statistical accuracy, momentum conservation has to be introduced by hand in several terms, especially in the square of the triple gluon vertex. Nevertheless, the algebraic complications are strongly reduced. Expectation values of the products of fields are thus obtained on lattices up to size $24^3 \times 32$.

Under the assumption that the bulk of the lattice artifacts is already removed[2] by using the variable $\hat{p}$ instead of p, the propagator up to 1-loop accuracy has the form

$$\hat{p'}^2 G(\hat{p'}^2) = 1 - g_0^2(\xi^{-1} c_1 \ln \hat{p'}^2 - c_2). \tag{20}$$

The standard SU(2)-result [14]

$$c_1 = \frac{\gamma_A^0}{16\pi^2} = \frac{13}{12}\frac{1}{4\pi^2} \tag{21}$$

is reproduced by the numerical procedure with good accuracy. The non-logarithmic term c_2, which is lattice-cut-off and action dependent has to be determined by numerical integrations. For anisotropic lattices, it depends on the direction of the momentum relative to the anisotropy. This leads to the different scale factors in space-like and time-like directions, introduced in eq. 18.

Up to 1-loop accuracy, it is ambiguous to rewrite eq. 20 in a scale-covariant form. This is so because the gluon propagator is multiplicatively renormalized by a g_0^2-dependent renormalization constant

$$Z_3(g_0^2) = 1 + z_2 g_0^2 + O(g_0^4). \tag{22}$$

We make the ansatz

$$\hat{p}^2 G(\hat{p}^2) = Z_3(g_0^2)[1 + \beta_0 g_0'^2 (\ln \hat{p}^2 - \frac{c_2'}{c_1})]^{-c_1/\beta_0} + O(g_0^6) \tag{23}$$

with

$$g_0'^2 = g_0^2/\xi, \;\; \beta_0 = \frac{22}{12}\frac{1}{4\pi^2}, \tag{24}$$

and get

$$c_2' = \xi(c_2 - z_2). \tag{25}$$

Rewriting this in terms of $\Lambda-$parameters, we have

$$\hat{p}^2 G(\hat{p}^2) = g'^{-2c_1/\beta_0}_0 Z_3(g_0^2)[\beta_0 \ln \hat{p}^2 \Lambda_{latt}^{-2} \Lambda_{prop}^{-2}]^{-c_1/\beta_0} \tag{26}$$

with

$$\Lambda_{latt}^2 = exp(-1/\beta_0 g_0^2), \;\; \Lambda_{prop}^2 = exp(c_2'/c_1). \tag{27}$$

[2]This holds on tree-level identically, and to one-loop accuracy on the level of 1% up to momenta of $a\hat{p} \leq 1.5$, according to the calculations described above.

More generally we can write eq. 26 in terms of the Λ_{prop}-dependent running coupling, constant, $g^2(p^2)$, as

$$\hat{p}^2 G(\hat{p}^2) = Z_3(g_0^2) g_0^{2c_1/\beta_0} g^2(\hat{p}^2)^{c_1/\beta_0}. \tag{28}$$

Here the running coupling constant will be inserted up to two-loop accuracy. The parameter Λ_{prop} will preliminarily be determined under the assumption $z_2 = 0$, and possible modifications will be discussed later in connection with Monte Carlo data at large β. On various isotropic lattices the method described above yields

$$c_2 = 0.1725 \pm 0.0004 \tag{29}$$

and

$$\Lambda_{prop} = 23.20 \pm 0.15. \tag{30}$$

The ensuing two-loop expression 28 will be compared to the Monte Carlo results in section 4, and very small differences will be found for large β and for momenta in the order of $a\hat{p} \approx 1.5$. For smaller momenta, agreement between Monte Carlo data and expression 28 becomes progressively worse.

We now turn to the anisotropic case. The non-logarithmic term c_2 has been deduced from the momentum-space integration, choosing the external momentum either predominantly space-like or time-like. I will describe the results by a Λ_{prop}-parameter for purely space-like momenta and an additional time-scale factor for the connection $\{p_0, \vec{p}\} \to \hat{p}^2$. corrections. The scale for the spatial directions, obtained by choosing momenta with $\hat{p}_0^2 \ll \vec{\hat{p}}^2$, follows from

$$c_2(\xi^2 = 3/2) = 0.1473 \pm 0.0009 \tag{31}$$

as

$$\Lambda_{prop}(\xi^2 = 3/2) = 26.7 \pm 0.5. \tag{32}$$

Similarly,

$$c_2(\xi^2 = 2/3) = 0.1931 \pm 0.0010 \tag{33}$$

and

$$\Lambda_{prop}(\xi^2 = 2/3) = 17.7 \pm 0.4. \tag{34}$$

The relatively large errors are mainly systematic ones and have their origin in lattice artifacts. Since at large momenta only the logarithm of Λ_{prop} is relevant in the perturbative expansion of the propagator, these errors do not endanger a comparison between Monte Carlo data and perturbation theory in that region.

The extra scale parameters for the time-like direction, introduced in eq. 18, follow from the perturbative calculation of c_2 for momenta with $\hat{p}_0^2 \gg \vec{\hat{p}}^2$. The results are

$$\lambda_{st} = 1.072 \pm 0.008 \quad \text{and} \quad \lambda_{st} = 0.925 \pm 0.01 \tag{35}$$

for $\xi^2 = 3/2, \beta = 2.2$ and $\xi^2 = 2/3, \beta = 3.3$ resp. These scale factors can also be determined in an independent way from the Monte Carlo data directly, as shown in section 4.3.

3 Gauging Algorithms and the Gribov Problem

The Landau gauge on an isotropic lattice is defined by minimizing the function

$$F(U,g) = \frac{1}{4V}\sum_{x,\mu}(1 - \frac{tr}{2}\{g(x)U_\mu(x)g^{-1}(x+e_\mu)\}). \tag{36}$$

by local gauge transformations $g(x) \in \mathrm{SU}(2)$. The SU(2)-link variables U_μ have been defined in eq. 1. A necessary condition for an extremum is that the lattice divergence, as a vector in colour space, vanishes:

$$\Delta\vec{u}(x) \equiv \sum_\mu [\vec{u}_\mu(x) - \vec{u}_\mu(x-e_\mu)] = 0. \tag{37}$$

It is well known that on sufficiently large lattices there will exist many local minima of the function $F(U,g)$, for which eq. 37 is satisfied. This phenomenon is the lattice analogue to the Gribov problem [6] in the continuum case. There exist extensive studies [8] for the situation when one sits in the absolute minimum, but it is hopeless, at least in practice, to find this minimum on large lattices by numerical methods. Consequently, there can be no confidence that those expectation values of gauge dependent quantities, which are taken with respect to some ensemble of local minima, are in essential agreement with those (hypothetical ones) which are taken with respect to the absolute minima. At present, the only viable procedure is to study the dependence of expectation values on different gauging algorithms and on the value of the gauge function achieved by them, and possibly to understand the difference between differently gauged configurations. This task has been initiated in ref. [26] for the maximally abelian gauge, where indeed some dependence has been found. In the present investigation, no effects have shown up so far within rather high accuracy, albeit not on very large lattices. This is so because gauging is a slow and time consuming procedure, such that there exist not too many gauged configurations for the largest lattices, with consequences to statistical significance. The bulk of investigations is therefore restricted to lattice sizes between 12^4 and $16^3 \times 32$.

On such lattices, no significant dependence of the propagator on the gauging prescription has been found. Different Gribov copies were eventually generated by applying 4 different gauging algorithms. Before explaning the results, a short review of these algorithms is appropriate. Many algorithms are, of course, designed to achieve the fastest approach to the minimum of $F(U,g)$, with the exception of the Simulated Annealing algorithm (SA) to be discussed below, in which speed is sacrificed in favour of a more thorough search for the absolute minimum. A well known obstacle against fast convergence is critical slowing down, often connected with long wavelength modes on large lattices [27]. This seems not to be the dominant problem here. All algorithms (except SA which is slow anyhow) suffer from the problem of localized and metastable gauge defects, where the dominant contribution to the gradient, eq. 37, comes from a region with size of 2 or 3 lattice sites. These regions may be quasistable for 50 or even 100 iterations, on a level of the residual gauge defect, which may be close to the gauging accuracy cut-off (see below). The occurrence of such states determines the convergence rate, and their number and/or complexity clearly increases with lattice size.

3.1 Gauging Accuracy

I define a minimum by allowing a residual value of the squared gradient

$$\delta = \frac{1}{V} \sum_x [\Delta \vec{u}(x)]^2 \leq 10^{-7}. \tag{38}$$

This is of course not at the limit of machine precision. It has been observed for 10 configurations on the $32^3 \times 64$-lattice with $\beta = 2.2$, $\xi^2 = 3/2$ that lowering this limit by two decades normaly leads to a negligible change of the propagator. In 9 cases the propagator for the smallest momentum changed by less than 10^{-2}, and in one case by 10 %. This latter case is characterized by the occurence of a sudden increase in the gradient[3] after $\delta = 10^{-7}$ had been reached. Regarding this case as exceptional, one may conclude that the uncertainty in the propagator caused by insufficient iteration seems to be much smaller than the fluctuations between the results of well separated configurations, which span roughly a factor 2 at the smallest momentum. Since a much lower value of δ may lead to a substantial increase in computer time, the above limit is a solid compromise.

3.2 Two Local Overrelaxation Algorithms

The gauging is done iteratively on a checkerboard of lattice sites. One easily sees that local gauge transformations given by

$$g(x) = P\{g_0 - i\vec{\tau}\Delta\vec{u}(x)\}, \tag{39}$$

where $P\{G\}$ stands for SU(2)-normalization of G, and where

$$g_0 = \sum_{\mu=0,3} [u_{0,\mu}(x) + u_{0,\mu}(x - e_\mu)], \tag{40}$$

leads to the minimum of $F(U, g)$ for a given colour of the checkerboard. In the ensuing step for the other colour, one moves again away from this minimum.

In the so-called Los Alamos method (LA) for overrelaxation [28], gauging with the matrix 39 is applied only with a small probability $P_{LA} < 0.5$, whereas in the remaining number of steps gauging with matrix 39 is applied twice. The latter operation leaves $F(U, g)$ unchanged. The speed of convergence depends on P_{LA}.

In the so-called Cornell method [27], one chooses a gauge matrix $g_c(x)$ which depends on some parameter such that for small values of the parameter one performs a steepest descent for the gauge function eq. 36, and for a non-infinitesimal parameter a multiple of the infinitesimal gauge matrix is exponentiated. Here, I use a simpler variant by taking as a gauge matrix

$$g_c(x) = P\{a_0 - i\vec{\tau}\Delta\vec{u}(x)\} \tag{41}$$

with a constant value a_0. In the continuum limit and for infinitesimal deviations from Landau gauge, the choice of the parameter $a_0 = 8$ almost leads to the absolute minimum at site x, and for $a_0 < 8$ we encounter overrelaxation. In practice a reasonable choice is $a_0 \approx 5.0$. For much smaller values, the algorithm diverges. This form of overrelaxation does not preserve the gauge function exactly, i.e. occasionally one may be taken farther away from the minimum. Most likely this is irrelevant since the usefulnes of exclusive

[3] See subsection *Conjugate Gradient* for more information.

use of overrelaxation has been doubted [26] because of settling too quickly in the next minimum at hand.

The Cornell method requires, on the average, 1.5 times more iterations than LA. Since fast gauging is perhaps not optimal in view of the simulated annealing technique, to be discussed below, this property is not of obvious disadvantage.

3.3 Conjugate Gradient Algorithm

In view of the fact that gauging far from the continuum limit is a tightly coupled nonlocal problem, an algorithm may be profitable which searches for the gradient in full space (without a checkerboard sequence) and which avoids the lack of efficiency of the method of steepest descent [29]. The method of choice is the conjugate gradient algorithm (CG) in the form given by Polak and Ribiere [29], which is adequate for non-quadratic forms, since it allows recovery. The CG provides optimal directions along which the function should be minimized. Here this 'line minimization' is done with help of the quadratic approximation to the gauge function and not with the full gauge function. The quadratic approximation is given by the variation of $F(U,g)$ under small gauges,

$$\delta F(U,g) = \sum_x \vec{g}(x)\ \Delta\vec{u}(x) + \frac{1}{2}\vec{g}M_{FP}\vec{g} + O(g^3), \tag{42}$$

with the Fadeev-Popov matrix M_{FP}

$$\begin{aligned} \vec{g}M_{FP}\vec{g} \;\; = \;\; & \sum_x \sum_{\mu=0,3} \Big[(u_{0,\mu}(x) + u_{0,\mu}(x-e_\mu))\vec{g}^2(x) \\ & +2\vec{g}(x)\cdot\vec{u}_\mu(x)\times\vec{g}(x+e_\mu) - u_{0,\mu}(x)\ \vec{g}(x)\vec{g}(x+e_\mu)\Big]. \end{aligned} \tag{43}$$

The line minimization uses a matrix element $h\,M_{FP}\,h$ in the denominator, and the positivity of this matrix element is a necessary, but not sufficient condition for the positivity of the Fadeev-Popov operator[4]. Occasionally, the line minimization actually leads to an increase of the gauge function, as the quadratic approximation to the gauge function may fail substantially. This 'blow up' of the CG usually leads to a drastic reduction of $F(U,g)$ in the next few iterations, i.e. a profitable new direction in a region characterized by strongly nonlinear effects has been found.

3.4 Simulated Annealing

Instead of seeking the fastest approach to (some) minimum, the introduction of an additional noise with shrinking amplitude in the spirit of simulated annealing has been advocated repeatedly [30, 26]. A definite improvement vs. stochastic overrelaxation has been seen for SU(2) when searching for the maximally abelian gauge [26]. Following this reference, I have combined the LA-method with $P_{LA} = 0.2$, where the move towards the local minimum has been modified by adding a Gaussian noise around the local minima. The amplidude of this noise decreased exponentially with the number of sweeps such that it becomes negligible after 300 sweeps. Furthermore, the amplitude is larger for a flat local minimum than for a steep one. Unfortunately, no tuning of this prescription

[4]This positivity is usually regarded, together with the divergence condition, as a proper definition of the Landau gauge. There is no way to prove the positivity. It could happen that we just do not sample the direction of h where there is a negative contribution.

was possible since no improvement could be observed in comparison to the CG. The overall observations will be described later.

3.5 Fourier acceleration

Although Fourier acceleration is tedious to implement on a parallel computer, I have tested it from start, because it is believed to eliminate critical slowing down completely [27, 31]. Unfortunately, this does not work out in practice. For almost 'cold' configurations, the algorithm converges beautifully and is much faster than any of the others. For fully thermalized configurations, however, the algorithm suffers from the phenomenon of metastable, well localized gauge defects mentioned previously. In this case all Fourier components of the gradient are approximately of same size and change very slowly under iterations. The convergence of the algorithm down to the level of accuracy eq. 38 is then determined by the number of 'hot spots' and their speed of dispersion, for which Fourier expansion does not seem to be helpful. This phenomenon is different from usual critical slowing down, i.e. the slow convergence of low Fourier components occuring even in the free field case. Whether Fourier acceleration becomes effective for sufficiently small δ remains to be seen.

3.6 A Comparison of Algorithms

The four algorithms (excluding Fourier acceleration) described above have been compared, among others, on lattices of size 16^4 with $\beta = 2.5$ and $\xi^2 = 1$. When applying different algorithms to a given gauge orbit, one ends up in different minima in more than 50% of the cases, and the same is true for one algorithm, after applying different random gauges before searching for the minimum. When comparing two specific algorithms, especially SA vs. CG, the final values of the gauge function eq. 36 may be different up to 2%, but both signs of the difference occur apparantly at random. A possible systematic algorithmic dependence is thus a difference of large numbers and not so easy to be pinned down.

Specifically, the average of the absolute differences is approximately

$$\overline{\mid \Delta F(U,g) \mid} \approx 1.7 \times 10^{-4} \tag{44}$$

to be compared to the gauge function itself at the minimum, $F(U,g) = 0.1146$. On the other hand, the variance of the gauge function on those relatively small lattices is

$$\delta F(U,g) \equiv \sqrt{\overline{F(U,g)^2} - \overline{F(U,g)}^2} = 1.0 \times 10^{-3} \tag{45}$$

which is thus considerably larger than the absolute spread due to different gauging procedures. Because of this large variance, it is possible to observe correlations between the result for the propagator and the gauge function, both measured on the same configuration. In detail, when comparing the propagators for configurations with a smaller than average gauge function, $F(U,g) \leq \overline{F(U,g)}$, with the opposite case, one finds differences among small momentum space propagators of the order of 3 to 5 %. The gauge function thus is indeed a measure for disorder on the lattice. Since the variations in $F(U,g)$ due to different algorithms amounts only to 17% of the variance due to different gauge orbits, (see eqs. 44 and 45) , we would expect little influence on the propagator from algorithmic choices, even if there were differences in $\overline{F(U,g)}$ for

different algorithms. But the average of the differences has been found compatible with zero in all runs, with an upper limit (1 σ) of

$$\overline{\Delta F(U,g)} \leq 4 \times 10^{-5} \tag{46}$$

which is 3% of the variance. Correspondingly, no differences could be observed for the propagator results within the statistical errors, which are slightly smaller than 1%. Quite similar results have been found by analyzing 200 configurations on a lattice of size $16^3 \times 32$ at β= 2.5. The main difference was that now the probability to end up in essentially different minima, was close to 80 %.

Summarizing, a spread in the gauge function due to different algorithms is noticable for each configuration individually, but the average value of the spread is compatible with zero, and, judged from the observed correlation between $F(U,g)$ and the propagator, no effects on the expectation values are expected, nor have been seen any. Similar results hold for the comparison between other pairs of algorithms.

The upper limit for a difference due to gauging algorithms, eq. 46, should be set in relation of the number of links on the lattice which is 8×10^4. This means that the possible difference between two algorithms can be expressed by a difference in the trace (see eq. 36) by one unit for 3 or 5 links. This number is small compared to the average number of links for which the trace is negative, i.e. which are far from the continuum limit. There are around 30 such links per configuration. The differences in the gauge function are thus compatible with a minor fluctuation in the number of links with gauge functions in this unphysical region. It is therefore difficult to associate too much significance to the difference in gauge functions.

The situation on the largest lattices of the present study is not so clear. On a $80 * 48^3$ lattice, 14 configurations separated by 200 sweeps have been gauged both with SA and CG. For 11 configurations, the propagator at the smallest momentum is up to 50% larger for SA than for CG, which is hardly significant in view of the insufficient separation of the configuration in terms of sweeps. There is no visible correlation with the value of the gauge function found by the two algorithms[5]. There is also no effect for the propagator at the next higher momentum, which, according to fig. 2 in the next section, is still deeply in the crucial infrared region. Clearly more work is necessary on large lattices to look for significant differences, but at the moment there seems to be no motivation for using the somewhat slow SA algorithm. Consequently, the bulk of the data has been taken with the CG algorithm, which is nonlocal and thus able to escape complicated valleys.

4 Results for the Propagator

4.1 The Data

The largest lattices have been used in connection with the anisotropy factors $\xi^2 = 3/2$ with β= 2.2, and with $\xi^2 = 2/3$ with β= 3.3. There the propagator has been measured on lattices of size $48^3 \times 80$, and on $64^3 \times 32$ resp. and on smaller ones. These measurements have been performed on the Intel Paragon Parallel-Computer at the HLRZ of the KFA Jülich, with the configuration distributed in packages of 16^4 sites on 135

[5] In one case there is agreement between the gauge functions within an relative accuracy of $2 * 10^{-6}$, whereas the smallest momentum propagators disagree by a factor 1.4.

or 128 nodes resp. The highly optimized code described in [32] has been used, which leads to an efficiency close to 50%, including communication. Smaller lattices have been analyzed on the SP2 with 32 nodes at GMD, St. Augustin, and on a Pentium-Pro PC.

About 15.000 sweeps have been done with 1:6 mixture of overrelaxation and heatbath updates. The Landau gauging algorithm (mainly conjugate gradient) has been applied after 1.000 sweeps, with the gauging accuracy given by eq. 38. Then the $\vec{u}_\mu$-fields were Fourier-transformed. For small momenta, all propagator contributions belonging to the same $\vec{p}^2$ and p_0^2 were averaged and the result stored. Propagators at larger momenta have been collected by immediate binning. In total about 900 independent momenta have been collected for each lattice size and β. In the final analysis, all momenta but the smallest ones have been binned, assuming a linear behaviour of $\hat{p}'^2 G(\hat{p}'^2)$ in $\hat{p}'^2$. The errors determined by binning and the statistical errors were found to be consistent after inclusion of the scale factor λ_{st}, as mentioned at the end of section 2.3.

4.2 Overall Characteristics and Finite Size effects

I will use the case $\xi^2 = 3/2$ with $\beta = 2.2$ to illustrate the general behaviour of the propagator as well as the absence of severe finite size effects. The results from three lattices have been overlayed[6] in fig. 1, where the dimensionless quantity

$$F(\beta, \hat{p}^2) = \sqrt{\hat{p}^4 + \mu^4} G(\hat{p}^2) \tag{47}$$

is shown. The mass μ has been chosen such that the plotted functions stay approximately constant at small $\hat{p}$. It turns out to be quite small,

$$\mu \approx (0.142 \pm 0.005) a^{-1}, \tag{48}$$

such that for $a\hat{p} \geq 0.2$, the function $F(\beta, \hat{p}^2)$ is essentially the full propagator divided by the bare one[7]. The above quantity should approach unity not at the lattice cut-off but at the renormalization point Λ_{prop}.

One notices the following properties:

- At large momenta, $a\hat{p} \geq 1.0$, the propagator exceeds tree level perturbation theory by 50%. This is consistent with moderate one-loop and higher contributions.
- The rise towards small $a\hat{p}$, relative to the bare propagator $G_0(\hat{p^2})$, accelerates and then stops suddenly[8] around $\hat{p}_{to} \approx 0.25/a$. In the representation of the inverse propagator (without an additional factor $\hat{p}^2$) as a function of $a^2\hat{p}^2$, shown in fig. 2, there is no break but a strong curvature at small $a^2\hat{p}^2$. When I draw a tangent to the interpolating curve which passes through the origin, it touches the curve at $a^2\hat{p}^2 \approx 0.055 \pm 0.02$ This explains the break seen in the previous representation.
- Within the errors ($\approx 5\%$ at the smallest momenta and $< 1\%$ at large momenta) there are no indications of finite size effects, except of course for the absence of the smallest momentum data points for the smaller lattices.

[6] Here and in the following the prime is dropped for the squared momentum, eq. 18.

[7] As will be shown below it is easy to find functions which interpolate better in the small $\hat{p}$-region. This is achieved at the expense of a more complicated transition to the $1/\hat{p}^2$-behaviour (modulo logarithmic corrections) in the perturbative region.

[8] The momentum value of the breaking point is sufficiently larger than the mass term μ in eq. 47 to be insensitive to its value.

In fig. 2, it is worth observing that the value of $\hat{p}_{to}$ at which the propagator approximately increases as $1/\hat{p}^2$ (and less steeply for smaller $\hat{p}$), lies in a region where excellent overlap between lattices of different sizes has been observed. Thus even the smallish lattice of size $24^3 \times 48$ shows this levelling-off phenomenon. Since the ambiguities due to gauging should be much less severe on smaller lattices, the explanation of the non-singular behaviour of the propagator as a gauging artifact is not probable.

Finite size effects in the large momentum region have also been studied carefully in connection with calculations in the perturbative region, and none have been found on the level of less than 1%. Whether effects are observable at small momenta and at large β (apart from the cut-off) is not so easy to decide. A definite danger is the appearance of a long autocorrelation time (in computer sweeps) for the small momentum components of the propagator which make their reliable determination difficult.

The turn-over momentum $\hat{p}_{to} = 0.25/a$, when rescaled to the isotropic case and to $\beta = 2.7$, corresponds roughly to a mass of 0.9 GeV. This value is based on the determination of the string tension in pure SU(2) [34, 35]. The turnover mass is thus considerably larger than the $\Lambda-$parameters obtained in deep inelastic scattering.

The strong increase towards smaller momenta, as compared to the tree level propagator, superficially resembles the increase of the running coupling constant. This interpretation is doubtful since, according to eq. 28, the propagator increases only with the fractional power 0.59 of the running coupling constant, and higher orders contributions cannot be too large in view of the close agreement with the tree level propagator. It is tempting to associate the bulk of the strong increase with nonperturbative effects. More details for this will be given in the next subsection.

4.3 Perturbative Momentum Region

It is very interesting to compare the Monte Carlo data for $a^2\hat{p}^2 \sim 2$ with perturbative expansions. One can obtain information on the way how perturbative behaviour is approached, and an estimate of the renormalization constant Z_3 is possible for suffiently accurate data[9]. We will see, however, that rather small values of the bare coupling constant g_0^2 are needed in order to come close to the perturbative prediction eq. 28, at least on the level of 0.5% say. This statement is not only supported by observed overall deviations from the perturbative formula (these could be due to higher order terms) but *a fortiori* by the fast variation of these deviations, both as function of the bare coupling constant and as function of $a\hat{p}$.

Results have mainly been collected on isotropic lattices, i.e. with $\xi = 1$. They are at β= 2.4, 2.7, 3.0 and 3.3, taken on relatively small lattices, namely $24^3 * 48$. The Monte Carlo data will first be analysed under the assumption $Z_3 = 1$, which fixes Λ_{prop}, once the one-loop results are used.

In fig. 3 I show the propagator results, normalized to the tree level propagator $1./\hat{p}^2$. The dotted lines with sparsely inserted symbols are the corresponding two-loop expressions, given in eq. 28, for $Z_3 = 1$. One realizes that agreement with two-loop perturbation theory is good at large momenta for β= 3.3, on the level of 1%. The agreement deteriorates quickly for decreasing β and decreasing momenta.

The interpretation of the excess of Monte Carlo data vs. two-loop perturbation theory as a 3^{rd}-order effect in $\alpha(p^2)$ is not convincing, due to its strong β-dependence:

[9] These may be seen as a substitute for a 2-loop calculation.

it decreases by approximately a factor 3 per $\Delta\beta = 0.3$ at fixed (lattice) momentum. The same is true if the difference is considered for decreasing $\hat{p}$ at fixed β. Furthermore it has to be noted that the difference between the one-loop and the two-loop expression for the running coupling constant at the largest β is around 2% of the total result only, and it is therefore natural to assume that the next order is of little importance. This points towards an exponentially decreasing, nonperturbative contribution, $\sim exp(-\lambda/g^2)$. Such terms have been identified in the anaylsis of Wilson loops previously [33, 38]. Tus it is very likely that even at large β and at $a\hat{p} \approx 1$ we observe the small tail of a nonperturbative contribution.

Now, at $\beta \geq 3.0$, the difference between 2-loop perturbation theory and Monte Carlo data is sensitive to assumptions on the renormalization constant Z_3, as given in eqs. 25 and 27. Because of the previously mentioned small second order contribution of 2% we neclect perturbative 3-loop contributions. Agreement between the Monte Carlo data and perturbation theory is then optimal if Z_3 is slightly smaller than 1:

$$z_2 \approx -0.01 \pm 0.02. \tag{49}$$

The errors are defined such that for z_2 at the lower limit, the Monte Carlo data fall below the perturbative curves for $\beta \geq 3.0$, and at the upper limit the Monte Carlo data for $\beta \geq 3.0$ do not approach the perturbative curves in a way which is compatible with an exponential decay, i.e. they stay well above the curves even at the largest β.

The crucial point is then that for such small values of the perturbative coefficient z_2 the renormalization constant varies only by less than 1% if the bare coupling constant varies by 10%. The latter shift is approximately what is available for scaling tests, which will be presented in the next section.

Data at β= 3.6, which are not shown here, confirm that the propagator at large momenta, $a\hat{p} \geq 1.0$ converges to the 2-loop curve, with significant discrepancies remaining at smaller momenta. This implies that the convergence observed at smaller values of β is not accidental in the sense that the data simply cross the curves[10].

Data at large β have been taken also for anisotropic lattices, and the results are perfectly consistent with the above findings and with the scale parameters derived in section 2.3. A detailed comparison with perturbation theory requires the knowledg of the extra scale factors λ_{st}, defined in eq. 18, which here will be determined independently by minimizing the spread of propagator results at momenta with different orientation on the lattice. On the large lattices this yields

$$\begin{aligned} \lambda_{st}(\xi^2 = 3/2, \beta = 2.2) &= 1.067 \pm 0.013, \\ \lambda_{st}(\xi^2 = 2/3, \beta = 3.3) &= 0.900 \pm 0.015 \end{aligned} \tag{50}$$

These results are consistent with the perturbative determinantion given in eq. 35. At larger values of β, another analysis has been performed on a smaller lattice, leading to values of λ_{st} closer to unity. This is in agreement with the one-loop perturbative dependence.

4.4 Small Momentum Region

In the small momentum region, the general behaviour of the propagator can be summarized in three observations, which can essentially be read off the presentation of the

[10]The statistical errors at such large β require a careful treatment, however, especially because of possible autocorrelations due to the small volume.

inverse propagator in fig. 2:

- For $p^2 \to 0$ the propapator definitely does not approach zero, as the inverse propagator decreases monotonously in this limit.
- An extrapolation of $G^{-1}(p^2)$ to a value of zero would require a rather complicated functional behaviour. The extrapolation to the value μ^2 (see eq. 47) looks quite natural in fig. 1.
- a linear interpolation of $G^{-1}(p^2)$ is not consistent for the lowest 4 data points within errors.

Clearly the detailed behaviour of the propagator at small momenta is extremely interesting, and phenomenological interpolation formulae may be helpful to establich trends. This will be persued in the next subsection.

4.4.1 Fitting a functional form

The functional behaviour of the propagator at small momenta has received considerable attention previously. It has been advocated in [20, 21] to analyze the propagator in terms of an anomalous dimension, eventually including a mass term. Such a fit of the form

$$G(\hat{p}^2) = const \left[M^2 + \hat{p}^2 \times \left(\frac{\hat{p}^2}{\Lambda^2_{latt}} \right)^{\eta} \right]^{-1} \tag{51}$$

works barely in the interval $0.0086 \leq a^2\hat{p}^2 \leq 0.35$ with $\eta \approx 0.43 \pm 0.03$, but not in momentum intervals extended towards larger $\hat{p}$. In [21], a value of $\eta = 0.532 \pm 0.012$ has been obtained for SU(3) in a somewhat higher interval of $\hat{p}^2$, namely $0.08 < \hat{p}^2 \leq 0.6$. If one tries to extend the validity of the interpolation formula to larger values of $\hat{p}^2$, one has to reduce the effective exponent of $\hat{p}^2$ to a value closer to 1.0, in agreement with an approach to perturbative corrections to the bare propagator. Similarly, in the smaller momentum interval plotted in fig. 2, a larger value of $\eta \approx 0.50$ gives the best fit, which is shown in fig. 2.

It might seem that the reasonable success of the above parametrization is an indication that the derivative of $G(\hat{p}^2)$ at $\hat{p}^2 = 0$ has zero slope. It is not possible to conclude this within present accuracy. In fact, a Gaussian parametrization with 2 parameters,

$$G(\hat{p}^2) = M^{-2} e^{-\hat{p}^2/\lambda^2}, \tag{52}$$

works well for the first 7 points, i.e. up to $\hat{p}^2 \approx 0.07 a^{-2}$, and it leads to a value of M^2 which is consistent with that from the previous parametrization, i.e. the extrapolations to $\hat{p}^2 = 0$ are mutually consistent. The resulting small value of λ,

$$\lambda \approx 0.2 a^{-1}, \tag{53}$$

is again a hint on the strong curvature of the inverse propagator.

5 Scaling

A necessary test for significance of the lattice result is scaling under a change of the bare coupling constant and of the action. The scaling of the dimensionless quantity $Z_3^{-1}\sqrt{\hat{p}^4 + \mu^4} G(\hat{p}^2)$ under a change of scale by a factor S can be read off eq. 28 as

$$\sqrt{\hat{p}^4 + \mu^4} G(\beta, \hat{p}^2) = \frac{Z_3(\beta)}{Z_3(\beta')} \sqrt{\hat{p'}^4 + S^4\mu^4} G(\beta', \hat{p'}^2) \tag{54}$$

with

$$\beta \to \beta', \;\; \hat{p}^2 \to \hat{p'}^2 = S^2 \hat{p}^2. \tag{55}$$

To anticipate the conclusions, the data show scaling to a good degree, and even perturbative scaling works reasonably well. A quantitative analysis has to cope with the uncertainties due to the unknown renormalization constant $Z_3(\beta)$ and to lattice artifacts. In the following I will use the conclusion of the study in the perturbative region (section 4.3):

- The renormalization constant is very close to 1, with the option to be slightly smaller than 1, i.e. $z_2 < 0$..
- Lattice artifacts are suffiently corrected for by using the variable $\hat{p}^2$ along the spatial directions.
- The scale factor λ_{st} between the spatial directions and the time-like direction can be calculated by one loop perturbation theory or by minimizing the scatter between propagators with momenta in different directions (see sections 20 and 4.3).

Then we find only minor violations of scaling between the small and large momentum regions. Asymptotic scaling is violated significantly, especially when the scaling match is enforced in the small momentum region.

5.1 Scaling for Fixed ξ

5.1.1 Scaling for $\xi^2 = 3/2$

The standard 2-loop perturbative result for the scale factor S under a change of β is

$$S(\beta = 2.0 \to 2.2)_{2-loop} = 1.857. \tag{56}$$

If one compares the propagators according to eq. 54 and with $Z_3 = 1$, there is reasonable agreement for $a\hat{p} > 0.8$. This is shown in fig. 4, where the data taken at β= 2.0 have been rescaled. Towards smaller momenta, however, the propagator for β= 2.0 shows at first a stronger increase, changing into a turning point at larger momentum such that it falls well below the propagator for $\beta = 2.0$ for $p \to 0$.

In order to get reasonable agreement in the region of the strong increase of the propagator one has to choose a significantly larger scale factor,

$$S(\beta = 2.0 \to 2.2)_{MC} \approx 2.1, \tag{57}$$

but such a choice still leads to considerable discrepancies. In order to obtain a good match one has to introduce a strong β-dependence of the renormalizion constant:

$$Z_3(\beta = 2.2)/Z_3(\beta = 2.0) = 1.07 \pm 0.02. \tag{58}$$

This finally leads to a scale factor

$$S(\beta = 2.0 \to 2.2)_{MC} \approx 2.24. \tag{59}$$

The resulting successful overlay of data is shown in fig. 5.

This discrepancy between perturbative and Monte Carlo scaling factors in the order of 20% is in agreement with several other determinations [38, 35]. It is of course an open question how the strong variation of Z_3 as a function of β can be explained in view of the fact that in lattice perturbation theory $Z_3 \approx 1$ within good accuracy. Here

we simply have to acknowledge that scaling works in a significantly different way for the nonperturbative contribution, which is responsible for the bulk of the propagator, compared with what perturbation theory suggests.

5.1.2 Scaling for $\xi^2 = 2/3$

The analysis for $\xi^2 = 2/3$ at the values of β= 3.1 and 3.3 leads to quite similar results. We get good agreement between the propagators at large momenta for the perturbative choice $Z_3 = 1$ and

$$S(\beta = 3.1 \to 3.3)_{2-loop} = 1.51 \tag{60}$$

with essentially the same discrepancies as above at smaller momenta. This is shown in fig. 6. Perfect overlap is achieved for

$$S(3.1 \to 3.3)_{MC} \approx 1.70, \tag{61}$$

and

$$Z_3(\beta = 3.3)/Z_3(\beta = 3.1) = 1.06 \pm 0.02. \tag{62}$$

It has to be noted that the change in scale is somewhat smaller here as in the previous case.

5.2 Scaling for Different ξ

Finally we analyze scaling of the propagators between the cases $\xi^2 = 3/2$ and $\xi^2 = 2/3$, on the largest lattices, at β-values β= 2.2 and β= 3.3 resp. Here the bare lattice Λ-parameters are equal due to the special choice of ξ^2 and β, but the propagator-scale-parameters Λ_{prop} are different of course. The ratio of these parameters can be calculated, again under the assumption $Z_3 = 1$, both by one-loop perturbation theory and by Monte Carlo simulation at high β. The result of the simulation is

$$\Lambda_{prop}(\xi^2 = 3/2)/\Lambda_{prop}(\xi^2 = 2/3) = 0.71 \pm 0.02, \tag{63}$$

and the perturbative calculation gives

$$\Lambda_{prop}(\xi^2 = 3/2)/\Lambda_{prop}(\xi^2 = 2/3) = 0.661 \pm 0.023, \tag{64}$$

pointing towards a minor discrepancy.

A comparison of the two anisotropic cases with such scale ratios leads to large discrepancies, and the data require a significantly larger ratio,

$$\Lambda_{prop}(\xi^2 = 3/2)/\Lambda_{prop}(\xi^2 = 2/3) = 0.77 \pm 0.01 \tag{65}$$

if agreement is demanded at large momenta. In fig. 7 the comparison is given with this ratio of Λ_{prop}-parameters. Obviously, one observes similar discrepancies at smaller momenta as in the previous cases, and a satisfactory matching requires again a variation of the renormalization constant. Thus, for

$$Z_3(\xi^2 = 3/2)/Z_3(\xi^2 = 2/3) = 1.040 \pm 0.007 \tag{66}$$

and

$$\Lambda_{prop}(\xi^2 = 3/2)/\Lambda_{prop}(\xi^2 = 2/3) = 0.90 \pm 0.003 \tag{67}$$

excellent agreement is achieved, which is shown in fig. 8.

5.3 Summary

In all the cases considered above and shown in figs. 4 to 8, there exist small but characteristic scaling violations in the sense that if the propagators belonging to different coupling constants or actions are matched at large momenta, the distribution at small momenta is broader in the case of larger coupling constants and at larger ξ. This holds if scaling factors are chosen close to the perturbative ones and if the renormalization factor Z_3 is taken as a constant, i.e. independent of β and of the anisotropy in the action. Allowing about 5% to 10% variation of this quantity is sufficient to remove the scaling violations to a high degree of accuracy. This strong variation of Z_3 could not be made plausible in perturbative calculations.

The case $\xi^2 = 2/3$ seems to be farther away from the continuum limit as the case $\xi^2 = 3/2$. This is at variance with the findings of [33]. One has to keep in mind, however, that the static potential analyzed in [33] receives contributions from all sorts of correlators, not just from the 2-point function.

In general one can state that the scaling properties of the propagator, especially deviations from asymptotic scaling, are in line with those observed in the static potential and in spectroscopy, and that possible variations in the shape of the propagator, especially some 'sharpening' of the peak at small p are small enough to give credence to the whole approach, which, in view of the Gribov problem, is not without uncertainties.

6 Visualization and the Stochastic Domain Picture

The suppression of long range correlations, relative to the perturbative behaviour, as indicated by an almost constant propagator at small $\hat{p}$, requires an interpretation. A valuable tool for this can be a visualization of the gauge fields in a given configuration. A picture of the gauge fields contains, in principle, more information than the 2-point function. The shape of possible domains, i.e. their surface structure, and the connection of different colour components can be read from a figure, but they are contained, on the numerical level, only in higher order propagators. Especially for the 3 colour components of SU(2) gauge theory, the colour facilities in modern computer graphics are quite useful.

Unfortunately the quantum noise, showing up in large fluctuations of the fields on the scale of one or 2 lattice units, is an obstacle for successful visualization at present values of β. There are two ways to overcome this. One is the well known cooling technique, where one applies several ($O(10)$) heatbath sweeps at large β to a given configuration. It is generally assumed that the long range structure of the gauge fields is unaltered by this procedure [36]. The other method is Fourier smoothing which has the advantage to leave intact the Landau gauge condition, i.e. the transverse property of momentum components. Here I have applied a 4-dimensional Fourier smoothing with a Gaussian filter,

$$F(\hat{p}) \sim e^{-\frac{1}{2}(\hat{p}_t^2+\hat{p}_x^2)-2(\hat{p}_y^2+\hat{p}_z^2)} \tag{68}$$

to the gauged configuration. Thus Fourier components of momentum $O(1)$ in the t,x-plane just start to suffer from filtering, whereas the filtering in the perpendicular directions (y,z) is stronger. In fig. 9 the first representation of the gluon fields on a lattice of size $48^3 \times 80$ is shown. All 3 SU(2)-colour components per lattice site are plotted[11]

[11] The picture has been generated by a lengthy VRML-program, which in turn was produced by a short FORTRAN

in the t, x-plane, with the cones indicating the orientation in three-dimensional x-space, i.e. the infomation from 3 links attached to one lattice site is included[12]. The size of the cones has been chosen proportional to the sum of squares of the amplitudes, corresponding to a 'hardening' of the picture.

The existence of domains is clearly visible in the sense that structures larger than than $10a$ do not show up. They are present, nevertheless, simply as fluctuations in the density of smaller domains. Stronger filtering would make such amplitudes visible, albeit with much reduced strengths. This, of course, is expressed quantitatively by the momentum space propagator. There is some tendency of clustering of different colours, but it remains to be seen in more than 2 dimensions whether this is statistically relevant. There is no indication for oscillating field distributions which one would expect to see in the free field case. It is of vital interest to follow the fields lines in the observed domains into the two 'missing' missing dimensions. Due to the Landau gauge condition, the divergence of the fields vanishes, and eventually flux tubes and/or vortices may be visible directly. After applying some cuts in the t, x-plane, this will be technically possible.

The domains appear relatively cleanly separated from each other by regions of low activity, but this impression is partly due to the 'hardening'. In a linear representation the domains are rather dense.

The visual impression thus leads to consider the physics of random domain formation. It is a natural consequence of this phenomenon that the propagator at zero momentum is finite, as can be seen as follows. Let us assume that a given lattice configuration is composed of randomly oriented domains of volume V_d with an average field strength $\overline{A}$. Then the zero wavelength Fourier component, which is $\sqrt{V}$ times the average field, is determined by a number of $N = \frac{V}{V_d}$ domains. Thus the variance of the total average is

$$\sigma[A(\hat{p}=0)] = \sqrt{\frac{V}{N}}\sqrt{\overline{A^2}} = \sqrt{V_d}\,\sqrt{\overline{A^2}}. \tag{69}$$

The zero momentum propagator is therefore a volume independent constant,

$$G(0) \approx V_d \overline{A^2}. \tag{70}$$

Eq. 70 can be checked qualitatively as follows. By averaging the squares of fields in the gauged configuration, I find $\overline{A^2} = 4.7 \times 10^{-3} a^{-2}$. On the other hand, from fig. 2 I deduce $G(0) \approx (200 \pm 20) a^2$, which leads to

$$V_d = G(0)/\overline{A^2} \approx 4.3 \times 10^4 a^4. \tag{71}$$

The resulting linear domain size of 14 lattice units is somewhat larger than the size of 10 lattice units, which can be read off fig. 9. But it has to be kept in mind that the extension in the y, z-directions is larger than in the t, x-plane which is shown. This due to the stronger filtering along the invisible directions. Further corrections are necessary for the regions with low activity, which can be recognized visually. On a qualitative level, therefore, agreement is satisfactory.

program.

[12] One direction has to be suppressed.

7 Discussion and Conclusions

In this paper the gluon propagator in SU(2) pure lattice gauge theory has been studied on fairly large lattices. The important overall results are:

- Absence of strong finite size effects, down to the lattice-size cut-off in momentum space, with twisted boundary conditions.
- The propagator approaches the 2-loop perturbative expression at $\beta \geq 3.0$ and at large momenta, if the renormalization constant is chosen very close to 1. For smaller momenta, $a\hat{p} < 1$, characteristic, rapidely increasing deviations survive even at the largest β investigated in this study. These are interpreted as nonperturbative effects.
- An increase of maximally a factor 4 with respect to the tree-level propagator is observed towards small momenta.
- A rapid departure downward, with respect to the previous trend, occurs at a physical momentum of about 0.9 GeV. This transition point is well within the region where finite size effects are excluded with high precision, and where artifacts due to non-unique gauging are extremely unlikely.
- A clearly nonlinear behaviour of the inverse propagator for $\hat{p}^2 \to 0$ is observed, with an extrapolation to a finite and nonzero value.
- The departures from asymtotic scaling under variation of the bare coupling constant are of the usual size, i.e. 20% departures for a change in scale by a factor 2.
- Approximate scaling holds with small, but characteristic departures between the small and large momentum region in all cases. These can be removed at the expense of a surprisingly strong variation of the renormalization constant Z_3.
- There is visual indication for domain formation. The domains seem to be dense in x-space and, when different colour components are superimposed, they seem to cluster.

To my knowledge, this is the first time that a dynamical quantity in nonabelian gauge theory has be monitored continuously from the perturbative region to the infrared region. Progressing in this direction, there is at first a smooth departure from perturbation theory which accelerates. It ends at a clear transition point, where a radically new behaviour sets in.

Accepting the existence of essentially randomly oriented domains, a crucial question concerns the details of the transition region. It could be that the field orientation of a domain does not penetrate deeply into the neighbouring domains, which would imply that the decrease of the correlation across the boundaries could be faster than exponential. In this respect, the analysis of previous investigations with excellent statistics [21, 37] clearly shows that the decrease in time t of the propagator in mixed coordinates, i.e. of $G(t, \vec{p})$, is faster than exponential, within a certain region in t. For the momentum-space propagator, a faster-than-exponential decrease is equivalent to the absence of a pole or even of any singularities for negative $\hat{p}^2$. This is consistent with the strongly nonlinear behaviour[13] of G^{-1}.

It is to be expected that a Gaussian behaviour would rule out the possibility of a Wick rotation or the propagator, i.e. the continuation to Minkowski-space. For the

[13] We repeat that a Gaussian form gives a satisfactory description for small momenta.

determination of masses, coupling constants and other gauge invariant quantities from lattice Monte Carlo data, a Minkowski-space representation is not necessary. For a phenomenological description of confinement effects in high energy scattering experiments this is, however, not so clear. At least at present one has to talk about the propagation of quarks and gluons over a certain distance for a short time.

I believe that the evidence for domain formation in the above sense is strong enough to justify further investigations along the following lines:

- What are the higher order correlations of momentum space amplitudes? These must be present in order to lead to well defined domains (in contrast to a simple suppression of small wavelength modes).
- The perturbative region has to be studied more carefully, especially on larger lattices in order to avoid freezing of the lattice configurations with huge autocorrelation times.
- Visualization has to be extended to field strengths $F^a_{\mu\nu}(x)$ and other dynamical variables.

Acknowledgement

The bulk of the Monte Carlo simulations has been performed on the Intel Paragon supercomputer at the HLRZ and ZAM, KFA-Jülich. The author is grateful to the HLRZ for granting computer time on the Paragon and on the SP2 with 32 nodes at GMD, St. Augustin, where smaller lattices have been analyzed. The help of the operating teams of ZAM and GMD has been indispensible, especially in getting along with the large amount of stored data.

Useful discussions with R.L. Stuller are gratefully acknowledged. Thanks are due to him and to H. Joos for a careful reading of the manuscript.

References

[1] R.L. Stuller, Phys. Rev. **D13** (1976) 513

[2] S. Mandelstam, Phys. Rev. **D20** (1979) 3223

[3] M. Baker, J.S. Ball and F. Zachariasen, Nucl. Phys. **B 181** 531 and 560.

[4] K. Büttner and M.R. Pennington, Phys. Rev. **D 52** (1995) 5220

[5] U. Ellwanger, M. Hirsch and A. Weber, LPTHE Orsay 96-50, HD-THEP-96-21, ICN-UNAM-96-08, (preprint 1996)

[6] S. Gribov, Nucl. Phys. **B139** (1978) 1

[7] M. Stingl, Phys. Rev. **D34** (1986) 3863

[8] D. Zwanziger, Nucl. Phys. **B 378** (1992) 525

[9] J. Ambjorn and P. Olesen, Nucl. Phys. **B 170** (1980) 60

[10] H.G. Dosch and Yu.A. Simonov, Physics Lett. **B 205** (1988) 339

[11] P.V. Landshoff and O. Nachtmann, Z. Physik **C35** (1987) 405

[12] UKQCD Collaboration, D.S. Henty, C. Parinello and D.G. Richards, Phys. Rev. **D54** (1996) 6923

[13] D.J. Gross and F. Wilczek, Phys. Rev. Letters **30** (1973) 1343

[14] H.D. Politzer, Phys. Rev. Letters **30** (1973) 1346

[15] M.A. Shifman, A.I. Vainshtein and V.I. Zakharov, Nucl. Phys. **B 147** (1979) 385, 519

[16] E. Bagan and M.R. Pennington, Physics Lett. **B 220** (1989) 453

[17] J.E. Mandula and M. Ogilvie, Phys. Lett. **B 185** (1987) 127

[18] E. Marinari, C. Parinello and R. Ricci, Nucl Phys. B362 (1991), 487

[19] C. Bernard, C. Parinello and A. Soni, Nucl. Phys. **B** (Proc. Suppl.) 30, (1993) 535

[20] P. Marenzoni, G. Martinelli, N. Stella and M. Testa, Physics Letters **B 318** (1993), 511

[21] P. Marenzoni, G. Martinelli and M. Testa, Nucl. Phys. **B 455** (1995), 339

[22] U. Heller, F. Karsch, Nucl. Phys. **B251** (1985), 254

[23] D. Daniel, A. Gonzáles-Arroyo and C.P. Korthals Altes, Phys. Lett. **B251** (1990), 559, and references quoted therein.

[24] P. Weisz, R. Wohlert, Nucl. Phys. **B236** (1984), 397

[25] F. Karsch, Nucl. Phys. **B205**, (1982), 285

[26] G.S. Bali, V. Bornyakov, M. Müller-Preussker and K. Schilling, Phys. Rev. **D54** (1996) 2863

[27] C.T.H. Davies, G.G. Batrouni, G.R. Katz, A.S. Kronfeld, G.P. Lepage, K.G. Wilson, P. Rossi and B. Stvetitsky, Phys. Rev. D 37 (1988), 1581

[28] Ph. de Forcrand and R. Gupta, Nucl. Phys. B (Proc. Suppl.) 9 (1989) 516

[29] W.H. Press, B.P. Flannery, S.A. Teukolsky, W.T. Vetterling, Numerical Recipies in FORTRAN, 2nd ed., Cambridge University Press, Cambridge 1992

[30] A. Hulsebos, Nucl. Phys. B (Proc. Suppl.) 30 (1993) 539

[31] A. Cucchieri and T. Mendes, Nucl. Phys. **B 471** (1996), 263

[32] F.Gutbrod, N. Attig and M. Weber, Parallel Computing **22** (1996), 443

[33] P. Altevogt and F. Gutbrod, Nucl. Physics **B452** (1995) 649

[34] S.J. Perantonis and C. Michael, Nucl. Phys. **B** (Proc. Suppl.) 20, (1991) 177

[35] S.P. Booth, A. Hulsebos, A.C. Irving, A. McKerrel, C. Michael, P.S. Spencer and P.W. Stephenson, Nucl. Phys. **B394** (1993), 509

[36] A. Di Giacomo, M. Maggiore, S. Olejnik, Nucl. Phys. **B347** (1990) 441

[37] H. Aiso, M. Fukuda, T. Iwamiya, M. Mizutani, A. Nakamura, T. Nakamura, M. Yoshida Nucl. Phys. **B** (Proc. Suppl.) 42, (1995) 899

[38] F. Gutbrod, Z. Phys. **C 37**, (1987), 143

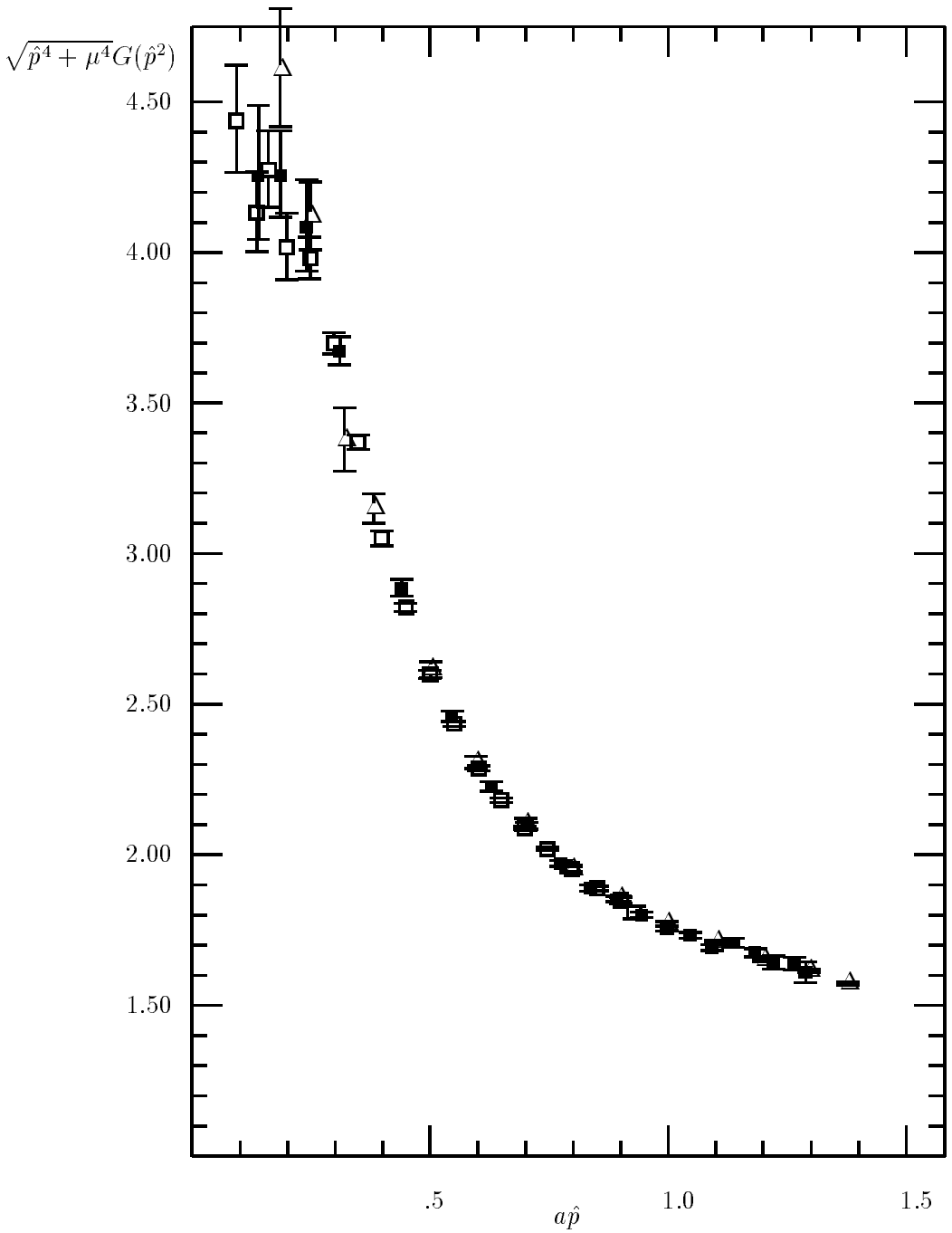

Figure 1: Gluon propagator $\times(\hat{p}^4+\mu^4)^{1/2}$ for $\beta = 2.2, \xi^2 = 3/2$, twisted b.c.. Lattice sizes are $24^3 \times 48$ (triangles), $32^3 \times 64$ (full squares) and $48^3 \times 80$ (open squares).

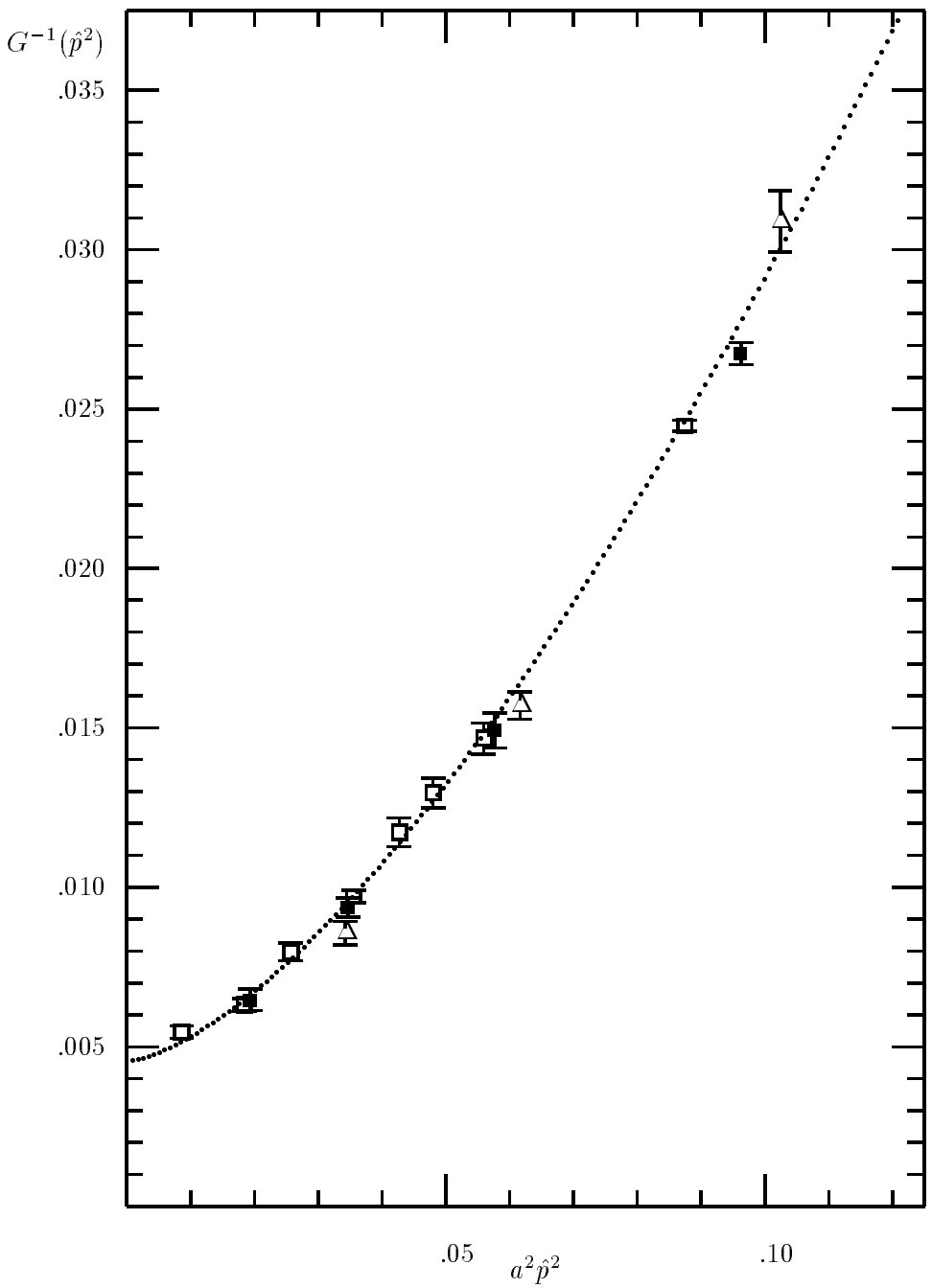

Figure 2: Inverse gluon propagator for $\beta = 2.2$, $\xi^2 = 3/2$, twisted b.c.. Lattice sizes are as in fig. 1. The dotted curve is the power-fit explained in section 4.4.1.

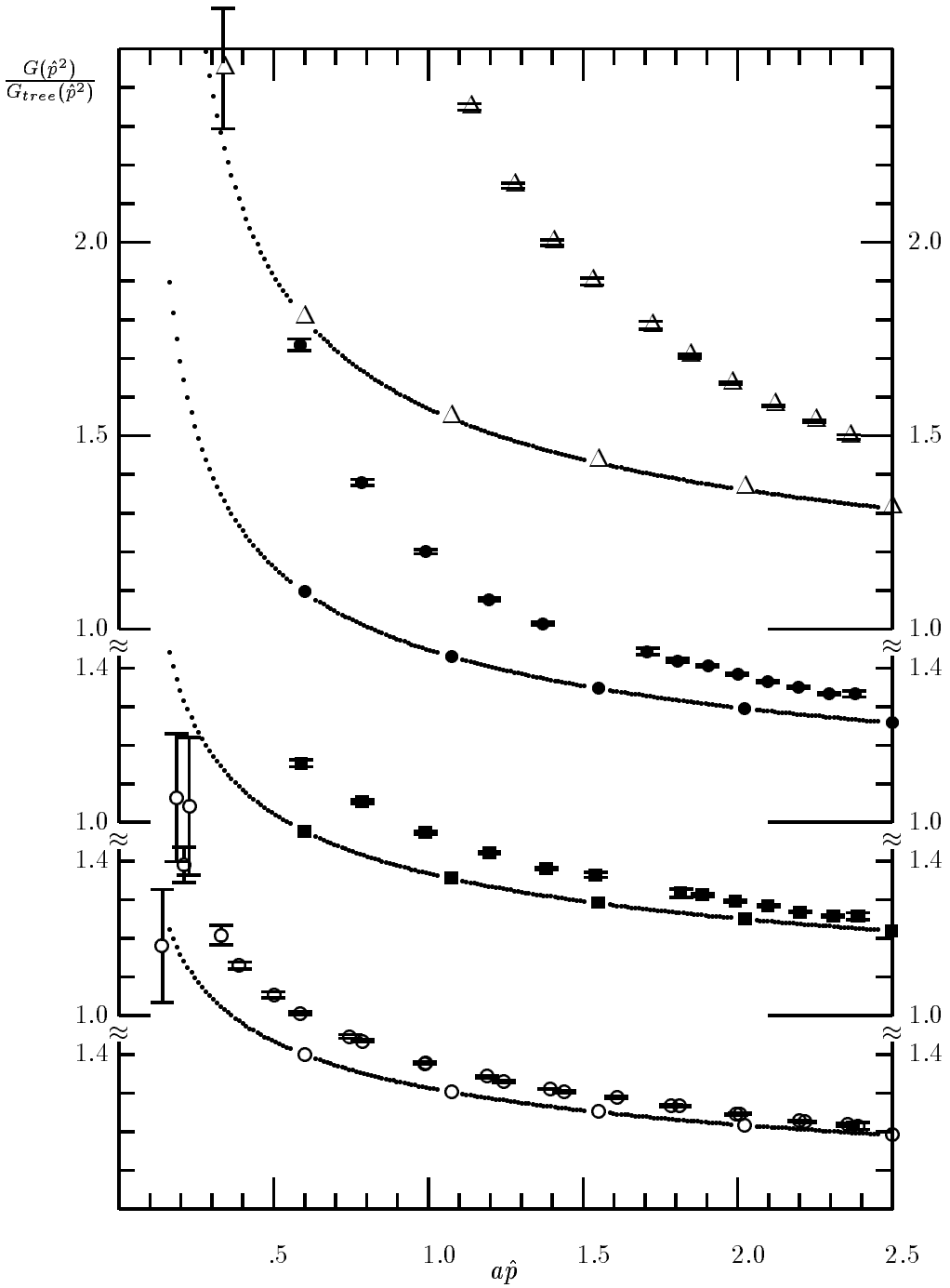

Figure 3: Gluon propagator compared to 2-loop perturbation theory, for $\beta = 2.4$ (triangles, upper curve), $\beta = 2.7$ (full circles, second curve from above), $\beta = 3.0$ (full squares) and $\beta = 3.3$ (open circles, lowest curve). Isotropic action, boundary conditions are twisted ones. Lattice size is $24^3 \times 48$.

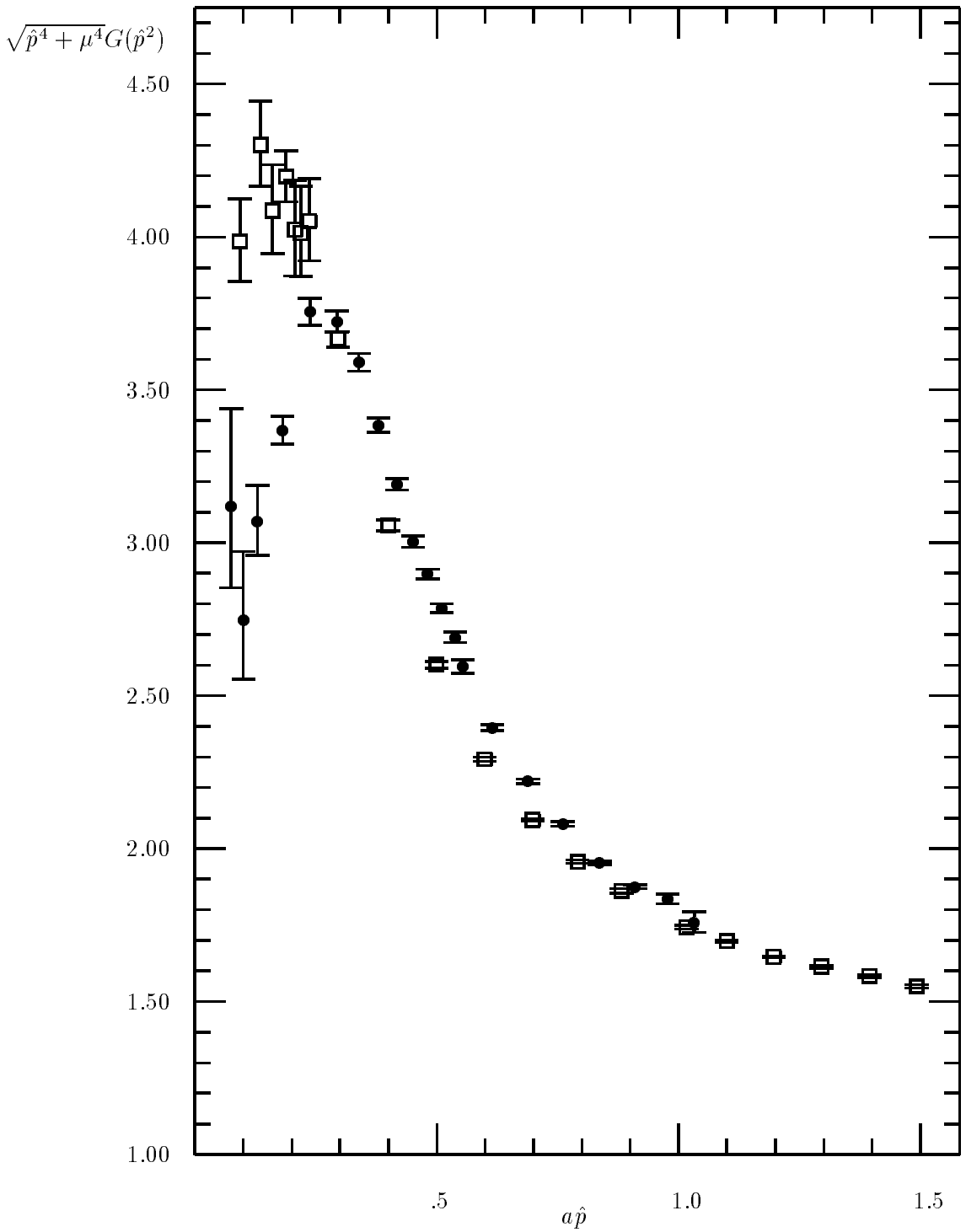

Figure 4: Scaling test: Propagator for $\beta = 2.2, \xi^2 = 3/2$ (open squares) vs. $\beta = 2.0$ (full circles). Lattice sizes are $48^3 \times 80$ and $32^3 \times 64$ resp.

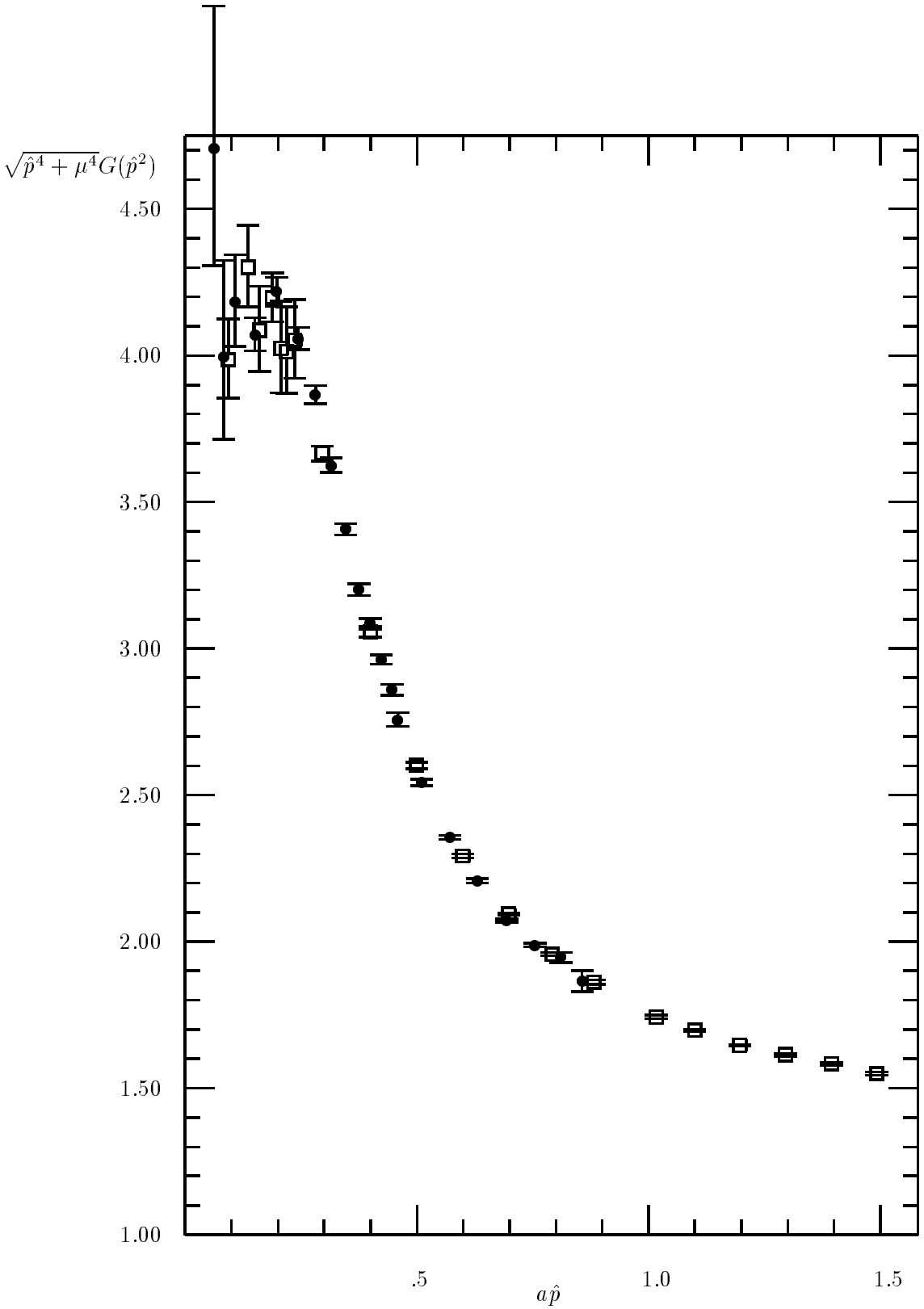

Figure 5: Scaling test: Propagator for $\beta = 2.2, \xi^2 = 3/2$ (open squares) vs. $\beta = 2.0$ (full circles). Lattice sizes are $48^3 \times 80$ and $32^3 \times 64$ resp.

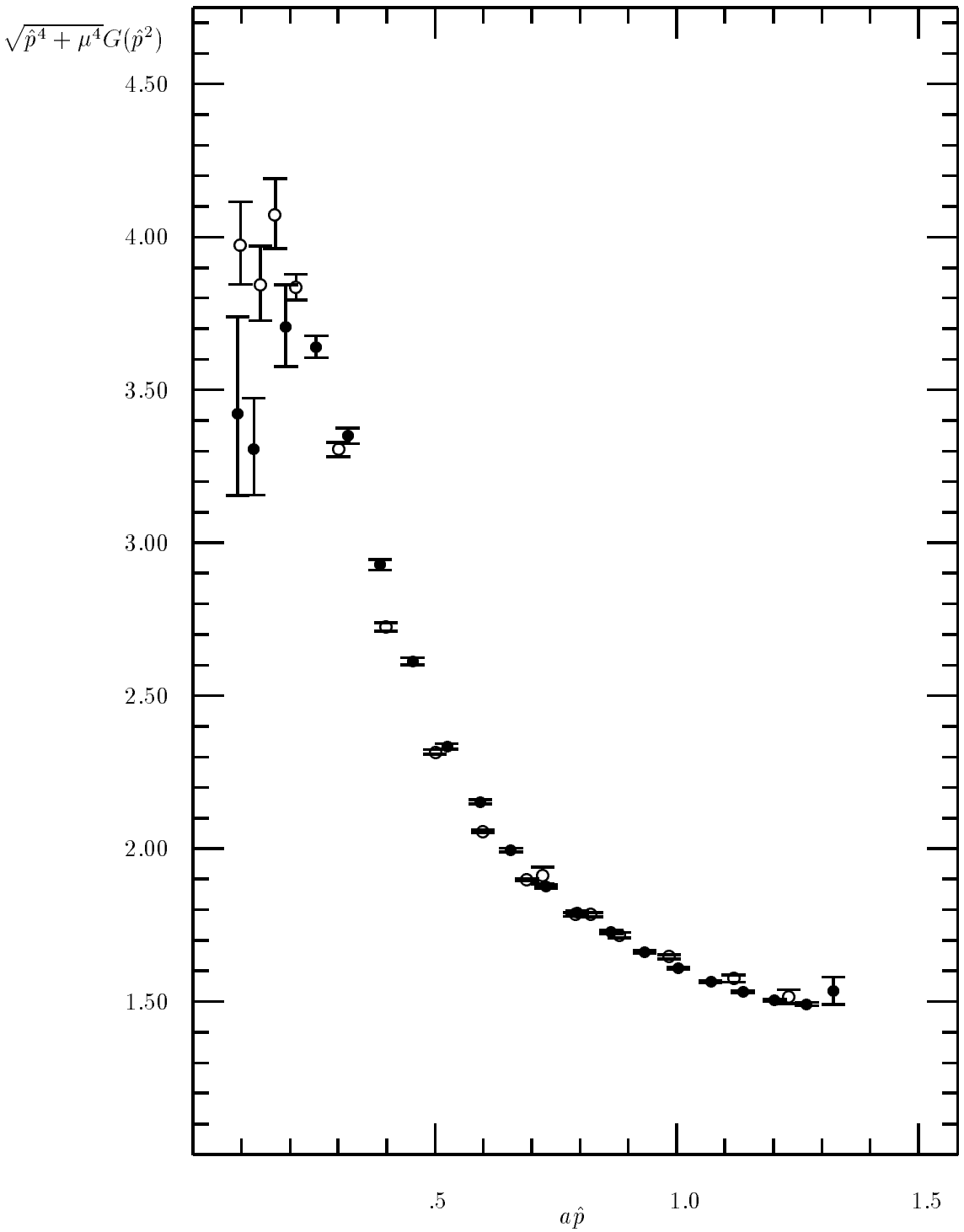

Figure 6: Scaling test: Propagator for $\beta = 3.3$, $\xi^2 = 2/3$ (open circles) vs. $\beta = 3.1$ (full circles). Lattice sizes are $64^3 \times 32$ and 32^4 resp.

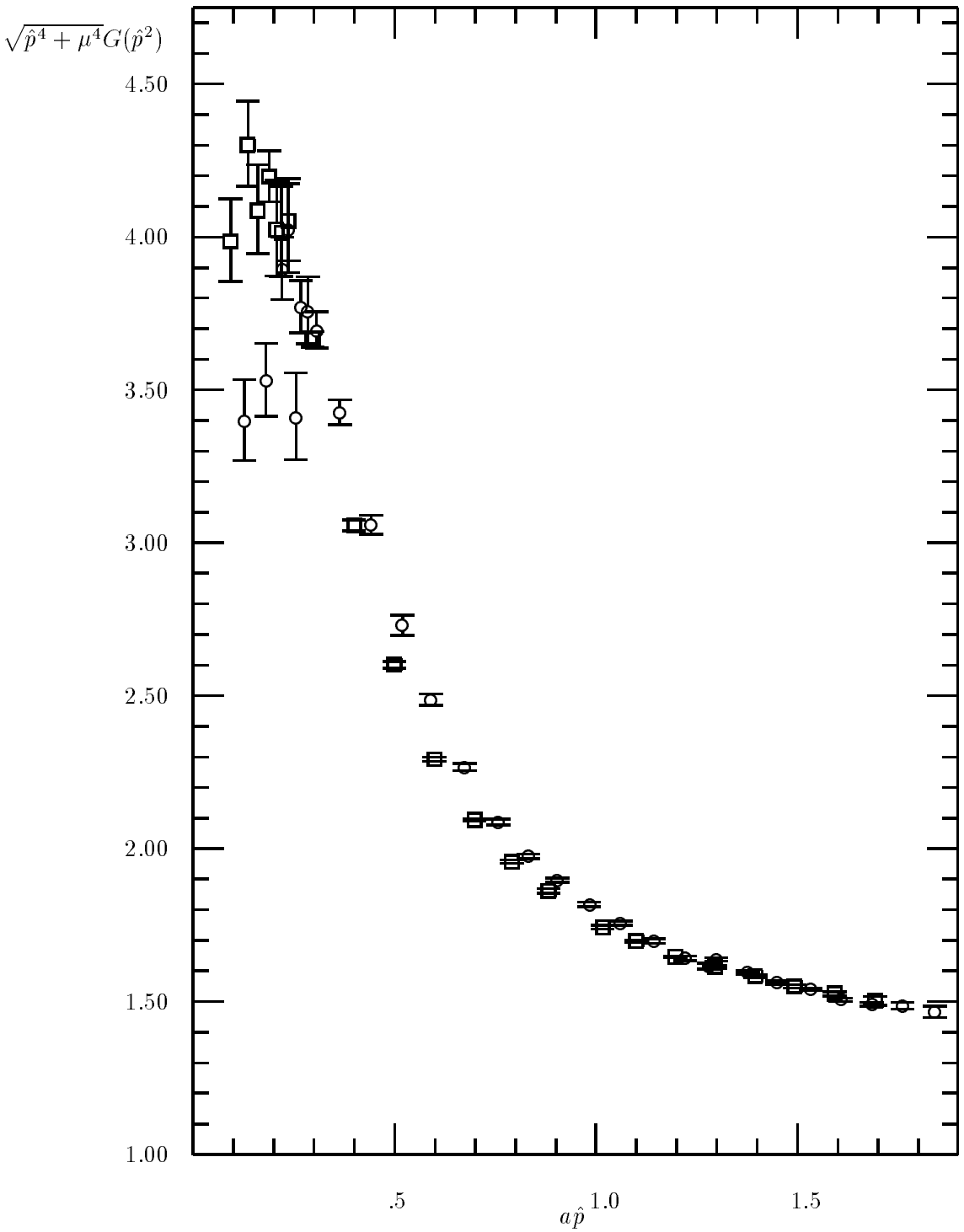

Figure 7: Scaling test: Propagator for $\beta = 2.2, \xi^2 = 3/2$ (open squares) vs. $\beta = 3.3$, $\xi^2 = 2/3$, (open circles). Lattice sizes are $48^3 \times 80$ and $64^3 \times 32$ resp.

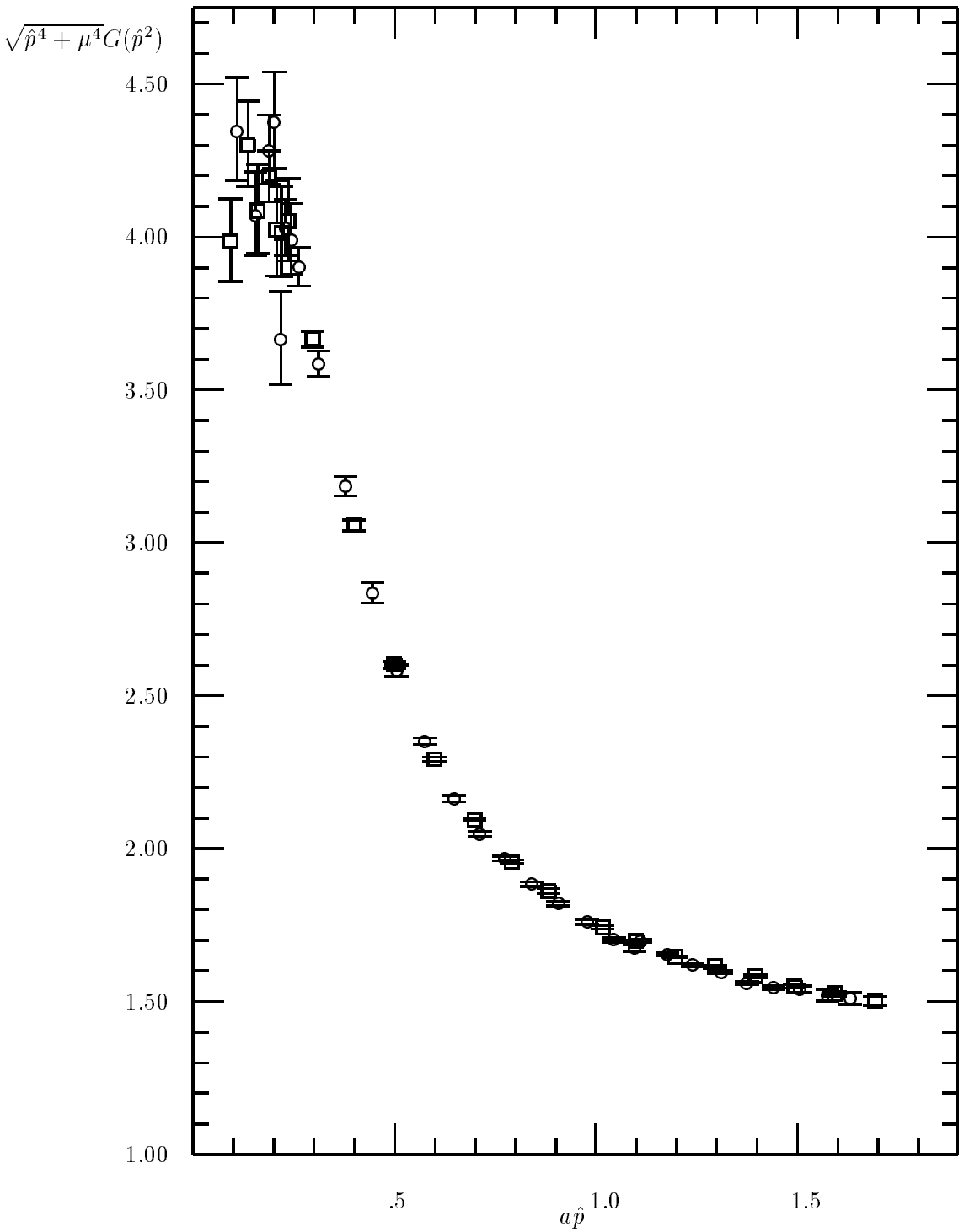

Figure 8: Scaling test: Propagator for $\beta = 2.2, \xi^2 = 3/2$ (open squares) vs. $\beta = 3.3$, $\xi^2 = 2/3$, (open circles). Lattice sizes are $48^3 \times 80$ and $64^3 \times 32$ resp.

Figure 9: Gluon field distribution in one plane of a $48^3 \times 80$ lattice, after Fourier smoothing.